

Magnetic structure of some rare-earth orthochromites

N. Shamir

Department of Physics, Nuclear Research Center-Negev, POB 9001, Beer Sheva, Israel

H. Shaked

*Department of Physics, Nuclear Research Center-Negev, POB 9001, Beer Sheva, Israel,
and Department of Physics, Ben Gurion University of the Negev, POB 653, Beer Sheva, Israel*

S. Shtrikman

Department of Electronics, The Weizmann Institute for Science, Rehovot, Israel

(Received 1 October 1980)

Neutron (2.4 \AA) elastic scattering measurements were conducted on $R\text{CrO}_3$ powder samples ($R = \text{Pr, Nd, Ho, Er, Tm, Yb, and Lu}$) whose magnetic structures were uncertain due to discrepancies between previous neutron scattering studies (which yielded nonaxial magnetic structures) and spontaneous magnetization and susceptibility studies (which yielded axial magnetic structures). The present neutron scattering measurements yielded axial magnetic structures for $R = \text{Pr, Nd, Ho, Er, Yb}$, in agreement with those obtained by magnetization and susceptibility. For PrCrO_3 , however, the Pr^{3+} magnetic moment obtained by the present neutron scattering study is significantly smaller than that obtained by magnetization studies. For the Pr and Nd compounds the direction of the magnetic moment was not determined due to lack of resolution. For TmCrO_3 the present neutron scattering spectra yielded temperature dependence of magnetic-reflection intensities that can be explained by a temperature-dependent aspherical spin distribution. With the use of this model the spectra are made consistent with an axial magnetic structure, in agreement with the magnetization and susceptibility results. For LuCrO_3 the present neutron scattering spectra resulted in a nonaxial structure in agreement with the previous neutron scattering studies. If we consider a temperature-independent aspherical spin distribution, these results can be made consistent with an axial structure, in agreement with the magnetization and susceptibility results. For $R = \text{Nd, Ho, Er}$ we find that the R^{3+} spin configuration has a sign opposite to that proposed by the previous neutron scattering, in agreement with the magnetization and susceptibility measurements. For these compounds it is also demonstrated that the R^{3+} magnetic order is induced by the Cr^{3+} sublattice. The latter result is in agreement with the magnetization and susceptibility studies and in disagreement with the cooperative ordering of the R^{3+} sublattice previously reported from neutron scattering studies of these compounds.

I. INTRODUCTION

The rare-earth orthochromites $R\text{CrO}_3$ (where R stands for a rare-earth metal) are isostructural with the rare-earth orthoferrites, $R\text{FeO}_3$, and crystallize in an orthorhombically distorted perovskite structure.¹ This structure belongs to the space group $D_{2h}^{16}-Pbnm$ with R in the (4c) and Cr in the (4b) positions as shown in Fig. 1. The possible magnetic configurations with symmetry isomorphic² to D_{2h}^{16} were defined by Wollan and Koehler³ and by Bertaut⁴ and are listed in Table I. The possible magnetic structures with symmetry isomorphic⁵ to D_{2h}^{16} have also been classified by Bertaut according to their magnetic symmetry, and this classification is given in Table II.

The orthochromites are paramagnetic at room temperature (RT) and are magnetically ordered at low temperatures.⁶⁻⁹ As these compounds are cooled

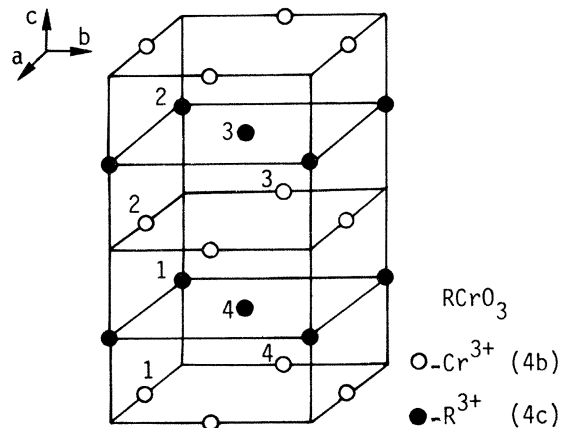


FIG. 1. Orthorhombic unit cell of $R\text{CrO}_3$. Only the R^{3+} (with position parameters $x=y=0$) and Cr^{3+} ions are shown.

TABLE I. Definition of magnetic-moment configurations (Refs. 3 and 4). The sites are numbered as in Fig. 1. The + means moment parallel to a particular direction, - means antiparallel to the same direction.

Configuration designation	Site			
	1	2	3	4
<i>F</i>	+	+	+	+
<i>G</i>	+	-	+	-
<i>A</i>	+	-	-	+
<i>C</i>	+	+	-	-

down from RT, the Cr sublattice is first to order at T_{N1} . This is a critical temperature and it decreases monotonically across the periodic table from 282 K in LaCrO_3 to 112 K in LuCrO_3 .⁷ The *R* sublattice orders (paramagnetic *R* ions only) at much lower temperature, T_{N2} , generally below 20 K. These, however, are not critical temperatures (see discussion), their variation is not monotonic across the periodic table and their determination is somewhat ambiguous. The magnetic structures of the orthochromites had been determined by neutron-elastic-scattering (NES) measurements on powder samples.⁶⁻⁹ Spontaneous magnetization and susceptibility (SMS) measurements done later on single crystals¹⁰⁻¹⁶ yielded magnetic structures that for some *R* ions ($R = \text{Pr}$, Nd , Ho , Er , Tm , Yb , and Lu) were different from

TABLE II. Possible magnetic structures in the (4*b*) and (4*c*) positions in D_{2h}^{16} with symmetry isomorphic (Ref. 5) with D_{2h}^{16} (G_α with $\alpha = x, y, z$ designates a *G* configuration with the spin axis along *a*, *b*, *c*, respectively, etc.).

Space group	Site			(4 <i>b</i>) Cr			(4 <i>c</i>) R		
<i>Pbnm</i>	A_x	G_y	C_z	-	-	C_z			
<i>Pbn'm'</i>	F_x	C_y	G_z	F_x	C_y	-			
<i>Pb'nm'</i>	C_x	F_y	A_z	C_z	F_y	-			
<i>Pb'n'm</i>	G_x	A_y	F_z	-	-	F_z			
<i>Pb'n'm'</i>	-	-	-	G_x	A_y	-			
<i>Pb'nm</i>	-	-	-	-	-	A_z			
<i>Pbn'm</i>	-	-	-	-	-	G_z			
<i>Pbnm'</i>	-	-	-	A_x	G_y	-			

TABLE III. The contribution to the two doublets (see text) of the magnetic moment configurations *A*, *C*, *F*, and *G*. The corresponding structure factors are given in terms of $\Delta = (hx + ky)$, where *x* and *y* are the position parameters of *R*.

<i>hkl</i>	Cr	<i>R</i>	
010	<i>C</i>	<i>C</i>	<i>G</i>
100	<i>C</i>	<i>C</i>	<i>A</i>
011	<i>G</i>	<i>G</i>	<i>C</i>
101	<i>G</i>	<i>G</i>	<i>F</i>
Structure factor	4	$4 \cos \Delta$	$4 \sin \Delta$

the structures determined by NES. Furthermore, the SMS structures were consistent with Table II, whereas some of the NES structures were inconsistent with this table.

The magnetic structures are essentially determined in the NES study from the two doublets: {010,100} and {011,101}. The contributions to these doublets from the four magnetic configurations are given in Table III. The ratio $I(011)/I(101)$ is approximately equal to 3, $\frac{1}{3}$, and 1 for G_x , G_y , and G_z respectively, on the Cr sublattice. When *R* is ordered in a *G*, *C*, or *F* configuration the above ratios are not valid. A detailed calculation of these ratios is given in the Appendix. Good resolution between members of the doublets is essential to the unambiguous determination of the magnetic structure. The previous NES studies were performed mostly with ~ 1 or $1.2\text{-}\text{\AA}$ neutrons. A significant improvement in resolution can be obtained by using $2.4\text{-}\text{\AA}$ neutrons. We have hence decided to use 2.4 \AA in a NES study of those chromites for which the proposed NES magnetic structures disagreed with the SMS magnetic structures.

The present NES measurements were performed on powder samples at the IRR-2 reactor, Beer-Sheva.

II. MAGNETIC STRUCTURES

The ratios between the intensities of magnetic reflections I_I/I_{II} , I_{II}/I_{IV} , and I_{III}/I_{IV} (for convenience we label {010}, {100}, {011}, and {101}, respectively, by I, II, III, and IV in order of increasing scattering angle) were calculated using Eqs. (8a)–(11a) developed in the Appendix. A short-hand notation is used in specifying the magnetic structure; for example, a structure where Cr^{3+} has G_x and A_y components and R^{3+} has an F_z component is labeled [G_x, A_y, F_z]. The results of the calculations in the

Appendix are used extensively in the analysis of the observed data. The important results of the calculations are

(a) Without a sign ascribed to them, the components uniquely determine the magnetic space group but do not define the spin configuration uniquely. For example, the components G_z, F_x on Cr and C_y, F_x on R give $2^3 = 8$ different moment configurations $[G_z, \pm F_x; \pm C_y, \pm F_x]$ belonging to $Pbn'm'$. The + sign corresponds to the definitions in Table I.

(b) A nonzero intensity in the reflections $\{010\}$ and/or $\{100\}$ means ordering of the moments on the R sublattice [this is not generally correct, since a C configuration on the Cr sublattice also contributes to these reflections (Table III) but this configuration was not found].

(c) The moment configurations $[G_z; \pm C_y, \pm F_x]$ and $[G_x; \pm F_z]$ are excluded by a nonzero $\{010\}$ reflection.

(d) As the sample is cooled down, the onsets of ordering on the Cr sublattice at T_{N1} and at (a lower temperature) T_{N2} on the R sublattice are expected to be seen in the temperature dependence of the intensities of magnetic reflections. A magnetic reflection containing contributions from the Cr and R sublattices has the following temperature dependence. There is a sharp rise in intensity (upon cooling) at T_{N1} , which tends to level off at lower temperatures. When T_{N2} is reached, there is either an increase or a decrease in the intensity depending on the configuration and on the reflection (Fig. 4). This is followed by a relatively sharp leveling off due to saturation (Figs. 4 and 9). The values of the magnetic moments and position parameters are given in Table IV. The form factor values were derived from the calculations of Freeman and Watson¹⁷ and experimental data for Cr^{3+} (Ref. 18) and Ho^{3+} (Ref. 19). In Table V, the calculated intensity ratios are compared to the ratios observed in the RCrO_3 spectra, taken at several (arbitrarily chosen) temperatures (Figs. 3 and 5–8).

A. PrCrO_3

Previous neutron scattering studies^{7,9} yielded at 4.2 K the moment configuration $[G_x; F_z]$, while SMS studies¹⁴ yielded $[G_z, F_x; -C_y, -F_x]$. The doublet $\{\text{III}, \text{IV}\}$, which enables the determination of the direction of the axis of the magnetic moments,²¹ is unresolved with 2.4-Å neutron beam (Fig. 2). A beam of 3.6-Å neutrons also yielded (not shown) insufficient resolution. In our 2.4-Å neutron scattering measurement (Fig. 2), however, a weak $\{010\}$, $\{100\}$ reflection is observed. This identifies the magnetic structure as $C_y F_x$ or C_z for the Pr^{3+} system and therefore (by symmetry) $G_z F_x$ or G_y , respectively, for the Cr^{3+} system. Compatibility with the SMS measurement¹⁴ leads to $[G_z; -C_y, -F_x]$. The negative sign preceding C_y indicates that the y component on

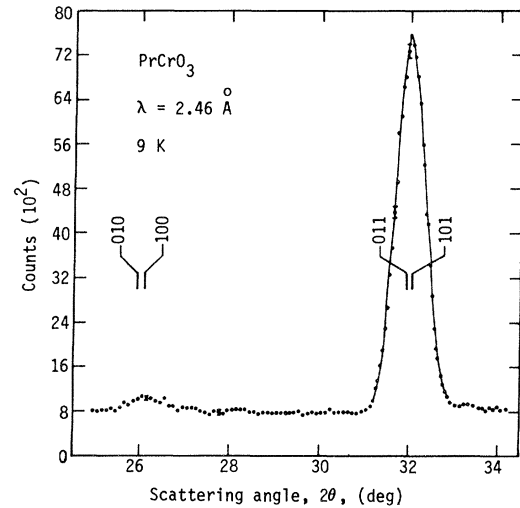


FIG. 2. NES spectrum of PrCrO_3 at 9 K. The solid line is only a guide to the eye.

the Pr^{3+} sites 1, 2, 3, 4 (Fig. 1) are $-, -, +, +$ (Table I), respectively. When the $\{011\}$ and $\{101\}$ reflections (III,IV) are resolved, the sign preceding the Pr^{3+} configuration is directly determined from the observed value and/or temperature dependence of $I_{\text{III}}/I_{\text{IV}}$ [see Sec. II C and Eqs. (A8), (A9), and (A10)]. However, assuming the value $2.2\mu_B$ for the Pr^{3+} magnetic moment and 47° as the angle of the Pr^{3+} moment to the y axis in the xy plane, as obtained by SMS measurements,¹⁴ the ratio $(I_{\text{I}} + I_{\text{II}})/(I_{\text{III}} + I_{\text{IV}})$ was calculated to be 0.44 compared to the observed value of 0.04. A detailed analysis shows that a $2.2\mu_B$ moment at any direction in the $[G_z; -C_y, -F_x]$ structure is inconsistent with the NES spectrum (Fig. 2). Assuming a $[G_y; \pm C_z]$ with a $2.2\mu_B$ Pr moment leads to ratios larger than 0.44. The observed intensities ratio can, therefore, be explained only when assuming a Pr^{3+} moment of about $0.6\mu_B$ (which is in agreement with the value, but not with the direction, of the moment obtained by previous NES measurements⁷). We have no explanation for the discrepancy between the NES and SMS results for the magnitude of the Pr^{3+} moment. A careful NES measurement on a single crystal (extinctions may raise a problem) may provide answers to this question.

B. NdCrO_3

Previous NES measurements⁷⁻⁹ determined the magnetic structure as $[G_x; -]$ (the long hyphen indicates a paramagnetic state of the Nd^{3+} ion) at 80 K and $[G_x 60^\circ; C_z]$ (the Cr^{3+} moment is 60° from the x axis) at 4.2 K. SMS measurements¹³ on the other hand yielded $[G_y; -C_z]$ at 4.2 K. The $\{011\}$ and $\{101\}$ pair (III,IV) was unresolved using 2.4-Å neu-

TABLE IV. The magnetic moments components in Bohr magnetons at 4.2 K and the position parameters of the R^{3+} ions, used in the calculations of intensity ratios presented in Table V. The uncertainties in the magnetic moments are about $\pm 0.2\mu_B$ for S^{Cr} and $0.6\mu_B$ (large S) to $0.3\mu_B$ (small S) for S^R , S^{Cr} , and S^R are correlated and the calculations fit within the errors in the observed data with these uncertainties.

R^{3+}	S^{Cr}	S_x^R	S_y^R	S_z^R	x^R	y^R
		0.38 ^a	0.35 ^a	0		
		-0.43 ^a	-0.40 ^a	0		
Pr	2.46 ^b	0	0	0.5 ^a	-0.010 ^c	0.035 ^c
		0	0	-0.6 ^a		
Nd	2.52 ^b	0	0	-1.93 ^a	-0.010 ^d	0.035 ^d
Ho	2.94 ^b	-3.4 ^b	-7.0 ^b	0	-0.015 ^a	0.043 ^a
Er	2.98 ^a	0	0	-4.62 ^a	-0.019 ^a	0.047 ^a
Tm	2.58 ^b	~0 ^a	-0.5 ^a	0	-0.020 ^c	0.048 ^c
Yb	2.80 ^b	-0.13 ^e	0	0	-0.020 ^c	0.049 ^c
Lu	2.51 ^b	0	0	0		

^a The present study, by best fit of the calculated to the observed intensity ratios.

^b Reference 7.

^c By extrapolation, and following the changes in position parameters of the R^{3+} ions in the orthoferrites. (Ref. 20).

^d Reference 8.

^e Reference 10.

TABLE V. Axial magnetic structures. Calculated magnetic intensity ratios I_I/I_{II} , I_{III}/I_{IV} , and I_{II}/I_{III} compared to the observed ratios in the present NES measurements. The position parameters and magnetic moments used in the calculations are those of Table IV. The sign of the configuration designation indicates the sign of the moments in site 1, for example $-C \equiv - - + +$.

R	Proposed mag. str. [Cr; R]	T (K)	I_I/I_{II}		I_{III}/I_{IV}		I_{II}/I_{III}	
			Obs.	Calc.	Obs.	Calc.	Obs.	Calc.
Pr	$[G_z, F_x; \pm C_y, \pm F_x]$	9	Unresolved	Unresolved	Unresolved	Unresolved	0.04 ± 0.01^a	0.04^a
	$[G_y; \pm C_z]$							
Nd	$[G_y; -C_z]$	4.2	Unresolved	Unresolved	Unresolved	0.34 ± 0.01^a	0.34^a	
Ho	$[G_z; -C_y, -F_x]$	90	1.08 ± 0.05	1.11	0	0
	$[G_z; -C_y, -F_x]$	4.2	0	0	2.96 ± 0.12	2.93	2.48 ± 0.04	2.47
Er	$[G_x; -F_z]$	35	3.39 ± 0.26	3.51	0	0
	$[G_y; -C_z]$	4.2	0.97 ± 0.02	0.96	2.11 ± 0.08	2.12	2.09 ± 0.04	2.09
Tm	$[G_z; -C_y, -F_x]$	100	1.08 ± 0.03	1.09	0	0
	$[G_z; -C_y, -F_x]$	77	...	0	1.19 ± 0.03	1.10	0	~0
	$[G_z; -C_y, -F_x]$	9	0	0	1.22 ± 0.02	1.13	0.03 ± 0.02	0.03
	$[G_z; -C_y, -F_x]$	5	0	0	1.24 ± 0.02	1.13	0.03 ± 0.02	0.03
Yb	$[G_z; -F_x]$	90	1.10 ± 0.09	1.09	0	0
	$[G_z; -F_x]$	4.2	1.12 ± 0.04	1.10	0	0
Lu	$[G_z; -]$	77	1.43 ± 0.04	1.10	0	0
		4.2	1.36 ± 0.04	1.10	0	0

^a For Pr and Nd we give in the last two columns the ratios $(I_I + I_{II})/(I_{II} + I_{IV})$ rather than I_{II}/I_{III} because we are unable to resolve the doublets $\{I, II\}$ and $\{III, IV\}$.

trons in the present NES study so the direction of the Cr^{3+} magnetic moment could not be determined by our measurement. As the sample was cooled down to 4.2 K, it was observed that $I_{\text{III}} + I_{\text{IV}}$ increased. This increase is consistent with $-C_z$ ordering of the Nd sublattice [Eq. (A9), notice that $+C_z$ will lead to a decrease]. Hence, $[G_y; -C_z]$ is the only structure which is consistent with the NES spectrum (Tables IV and V), its temperature dependence [Eq. (A9)] and symmetry (Table II), in full agreement with SMS results. The magnitude of the magnetic moment calculated from the observed ratio $(I_{\text{I}} + I_{\text{II}})/(I_{\text{III}} + I_{\text{IV}})$ using previously published^{7,8} S^{Cr} and position parameters (Table IV) is $|S^{\text{Nd}}| = 1.93 \mu_B$.

C. HoCrO_3

Previous NES measurements^{6,7} yielded $[G_{xy}86^\circ; -]$ at 80 K and $[G_z; C_y, F_x]$ at 4.2 K. The structure determined by SMS measurements¹¹ is $[G_z; -C_y, -F_x]$ for the whole temperature range. Our NES measurement (Fig. 3) yields $I_{\text{II}}/I_{\text{III}}$ and $I_{\text{III}}/I_{\text{IV}}$ which are in good agreement with the calculations assuming the $[G_z; -C_y - F_x]$ structure for both 90 and 4.2 K and using magnetic moments and position parameters within the error range of previous experimental determinations (Table IV). As the sample was cooled down, the $\{011\}$ (I_{III}) increased and the $\{101\}$ (I_{IV}) decreased (Fig. 4). This is consistent with $-C_y, -F_x$ ordering of the Ho sublattice [Eq. (A8), $\sin\Delta_{\text{III}} > 0$ and $\sin\Delta_{\text{IV}} < 0$]. A $[G_z; C_y, F_x]$ configuration will cause I_{III} to decrease and I_{IV} to in-

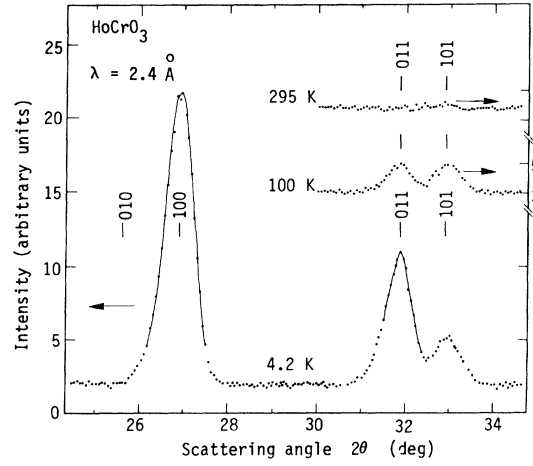


FIG. 3. NES spectra of HoCrO_3 at 4.2, 100, and 295 K.

crease in disagreement with the observed behavior. Furthermore, the temperature dependence of the square of the Ho moment is given by $(\sqrt{I_{\text{III}}} - 1.035\sqrt{I_{\text{IV}}})^2$ which is found to coincide with intensity-versus-temperature curve of the $\{100\}$ reflection.²³ Hence, $[G_z; -C_y, -F_x]$ is the only structure which is consistent with the neutron scattering spectrum at 4.2 K (Fig. 3, Table V), the observed temperature dependence [Fig. 4, Eq. (A8)] and symmetry (Table II). This determination is in complete agreement with the 4.2 K SMS structure¹¹ (Table VI).

TABLE VI. Summary of magnetic structures obtained by previous NES (Refs. 6–9) (NES 1) SMS (Refs. 10–16) and by the present NES (NES 2).

$R\text{CrO}_3$	80 K			4.2 K		
	NES 1	SMS	NES 2	NES 1	SMS	NES 2
PrCrO_3	$[G; -]$	$[G_z, F_x; -]$	$[G; -]$	$[G_x; F_z]$	$[G_z, F_x; -C_y, -F_x]$	$[G_z, F_x; \pm C_y, \pm F_x]$
NdCrO_3	$[G_x; -]$	$[G_x; -]$	$[G; -]$	$[G_{xy}60^\circ; C_z]$	$[G_y; -C_z]$	$[G_y; -C_z]$
HoCrO_3	$[G_{xz}86^\circ; -]$	$[G_z, F_x; -]$	$[G_z; -]$	$[G_z; C_y, F_x]$	$[G_z, F_x; -C_y, -G_x]$	$[G_z; -C_y, -F_x]$
ErCrO_3	$[G_x; -]$	$[G_x, F_z; -]$	$[G_x; -]$	$[G_{xy}47^\circ; C_z]$	$[G_y; -C_z]$	$[G_y; -C_z]$
TmCrO_3	$[G_{xz}62^\circ; -]$	$[G_z, F_x; -]$	$[G_z; -]$	$[G_x; F_z]$	$[G_z, F_x; -C_y, -F_x]$	$[G_z; -C_y, -F_x]$
		$[G_x, F_z; -]$			$[G_x, F_z; -F_z]$	
YbCrO_3	$[G_{xz}68^\circ; -]$	$[G_z, F_x; -F_x]$	$[G_z; -]$	$G_{xz}68^\circ; F_x]$	$[G_z, F_x; -F_x]$	$[G_z; -F_x]$
LuCrO_3	$[G_{xz}63^\circ; -]$	$[G_z, F_x; -]$	$[G_{xz}; -]$	$[G_{xz}63^\circ; -]$	$[G_z, F_x; -]$	$[G_{xz}; -]$

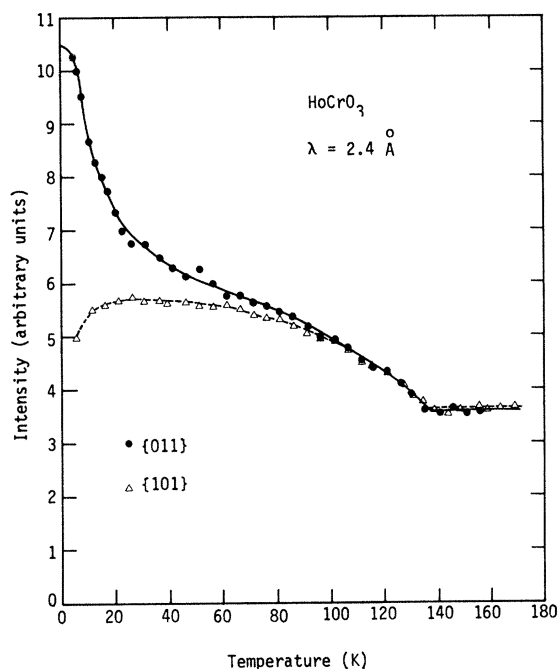


FIG. 4. Temperature dependence of the intensities of the magnetic reflections {011} and {101} (III and IV) for HoCrO_3 .

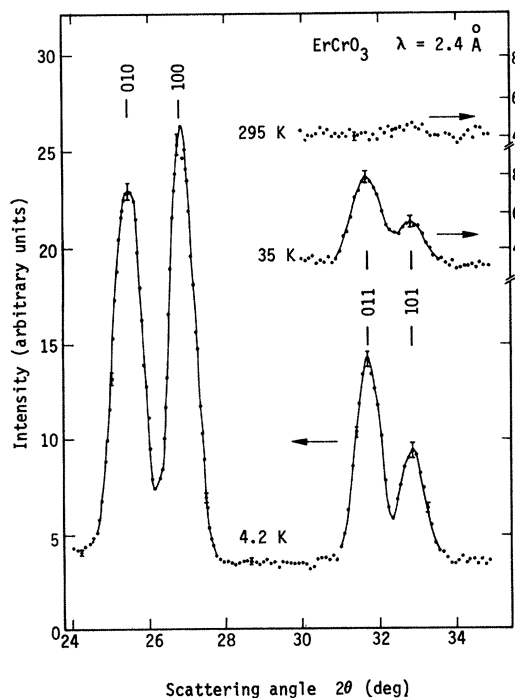


FIG. 5. NES spectra of ErCrO_3 at 4.2, 35, and 295 K.

D. ErCrO_3

Previous NES measurements⁷⁻⁹ yielded $[G_x; -]$ at 80 K and $[G_x, 47^\circ; C_z]$ at 4.2 K. The structure determined by SMS measurements¹⁵ is $[G_x, F_z; -]$ and $[G_y; -C_z]$ above and below 9.3 K, respectively. Our NES measurements (Fig. 5), yielded intensity ratios which are in good agreement (Table V), with the $[G_x; -F_z]$ structure above the transition temperature as agreed by all techniques^{7-9, 15} and $[G_y; -C_z]$ below the transition temperature [where the reflections {010} and {100} appear] in agreement with SMS measurements.¹⁵ Here too the Cr^{3+} system is in the $-C$ configuration relative to the Cr^{3+} system and not in C as indicated by the previous neutron scattering measurements.⁸ To give an idea, $[G_y; C_z]$ leads to a calculated $I_{\text{III}}/I_{\text{IV}} \sim 0.01$ whereas, the observed value is 2.11.

E. TmCrO_3

The magnetic structures obtained by previous neutron scattering measurements^{7, 9} are $[G_x, 62^\circ; -]$ and $[G_x, F_z]$ at 80 and 4.2 K, respectively. As a small external magnetic field is sufficient to rotate the Cr^{3+} moments from the x to z axis and vice versa the magnetic structure was not determined unambiguously by SMS measurements,¹² and the two structures $[G_x; -F_z]$ or $[G_z; -C_y - F_x]$ were found to be equally consistent with the SMS data. The NES spectra obtained in the present study (Fig. 6) are not fully understood. Let us consider symmetries and intensities.

(i) Symmetries. A weak {100} but no {010} reflection is observed at 4.2 K. This is consistent with a C_y structure on the Tm sublattice (Table III) and by symmetry (Table II) we deduce a $[G_z, \pm C_y, \pm F_x]$ structure.

(ii) Intensities. The temperature dependence of the {101} reflection (I_{IV}) is similar to that of LaCrO_3 , YCrO_3 , and LuCrO_3 . Hence it contains neither a contribution from Tm nor from a reorientation of the Cr^{3+} moment. On the other hand, the small $I_{\text{II}}/I_{\text{III}}$ value leads to a C_y (Tm) component which is too small to justify the observed change in the {011} reflection (I_{III}) with temperature (Fig. 6, bottom, $T/T_N < 0.3$). This disagreement comes out in the comparison between the observed and calculated $I_{\text{III}}/I_{\text{IV}}$ (Table V, $T = 77, 9, 5$ K). A possible explanation for this unusual temperature dependence of I_{III} is a temperature-dependent nonspherical spin distribution of the Cr^{3+} sublattice. This explanation was offered in the case of TmFeO_3 and YbFeO_3 where a similar temperature dependence of I_{III} and I_{IV} had been observed.²¹

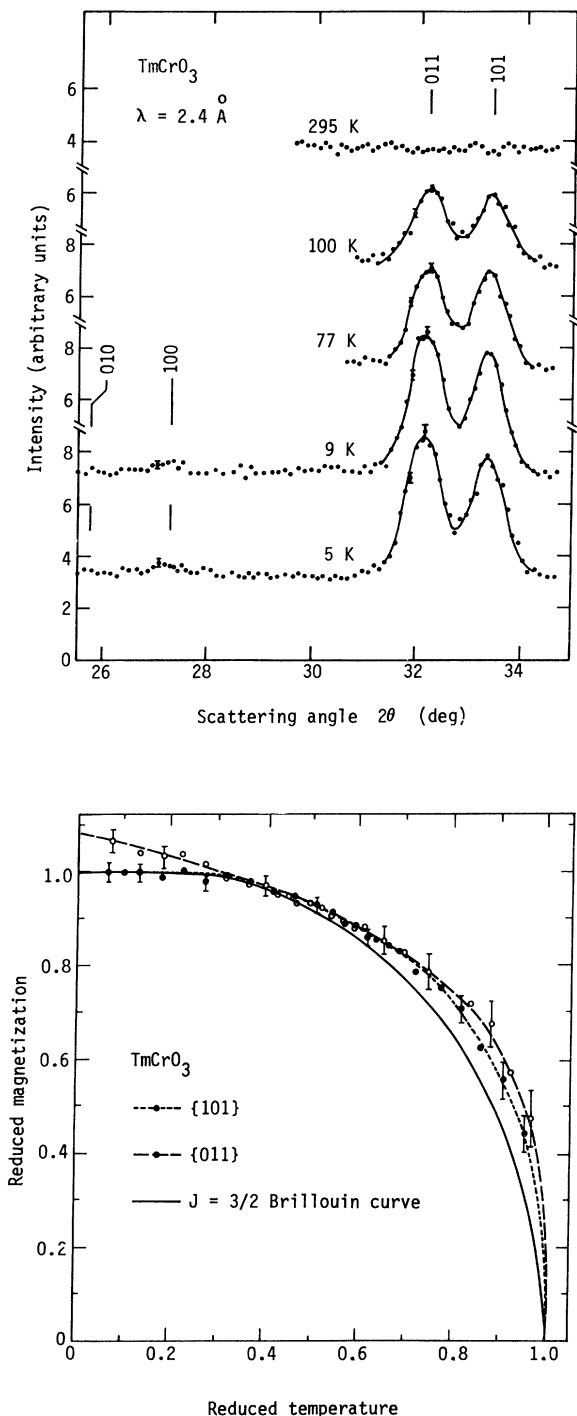


FIG. 6. Top: NES spectra of TmCrO_3 at 5, 9, 77, 100, and 295 K. Bottom: Reduced magnetization vs reduced temperature ($T_N = 124$ K) for the {011} and {101} (III and IV) reflections of TmCrO_3 , compared to the $J = \frac{3}{2}$ Brillouin curve. The {011} magnetization is scaled to unity at $T/T_N = 0.3$. The dashed curves are only guides to the eye.

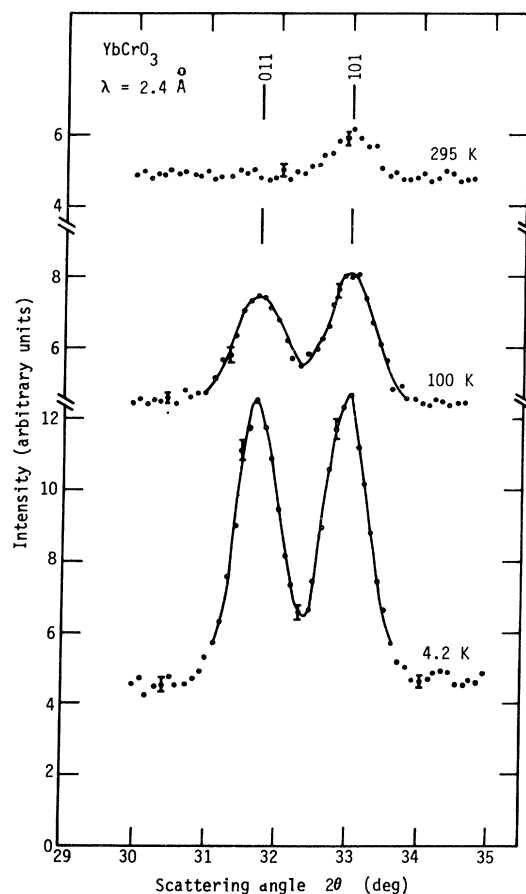


FIG. 7. NES spectra of YbCrO_3 at 4.2, 100, and 295 K.

F. YbCrO_3

The magnetic structures obtained by previous NES measurements^{7,9} are $[G_{xz}68^\circ; -]$ and $[G_{xz}68^\circ; F_x]$ at 80 and 4.2 K, respectively. SMS measurements yielded¹⁰ on the other hand $[G_z; -F_x]$ structure for the whole temperature range. Our NES measurements (Fig. 7) concur [Table V and Eq. (8a)] with the $[G_z; -F_x]$ structure.

G. LuCrO_3

The magnetic structure obtained by the previous NES measurements^{7,9} is $[G_{xz}63^\circ; -]$ for all temperatures below T_N . SMS measurements yielded¹⁶ on the other hand, $[G_z; -]$ at all temperatures of the ordered state. The present NES measurements (Fig. 8) yielded $I_{\text{III}}/I_{\text{IV}}$ which is neither consistent with G_z (Table V) nor with G_x . It seems that for LuCrO_3 the $G_{xz}63^\circ$ determination of the magnetic structure by the previous NES measurements is consistent with

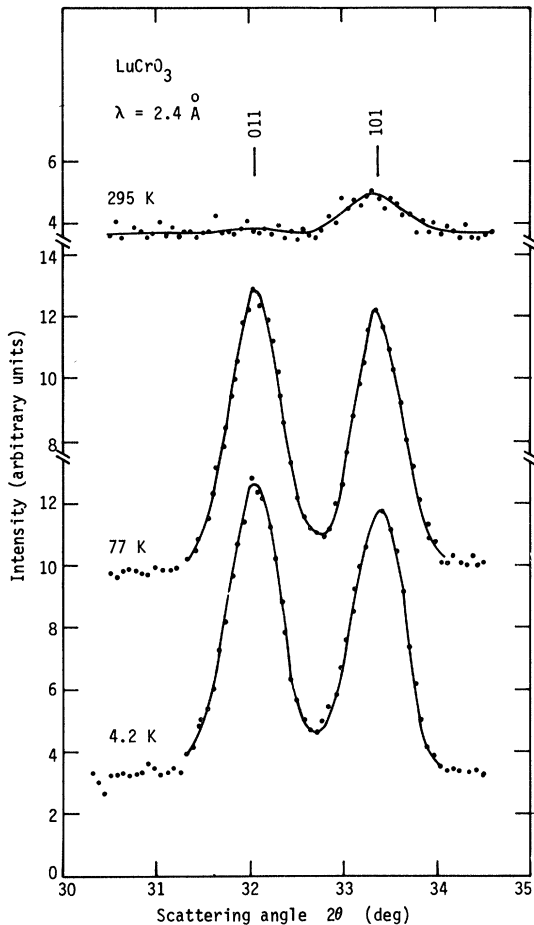


FIG. 8. NES spectra of LuCrO_3 at 4.2, 77, and 295 K.

our result. A possible way to make the NES and SMS structures consistent is to assume a temperature-independent nonspherical spin distribution for the Cr^{3+} ions.²¹

III. NATURE OF THE MAGNETIC ORDERING OF R^{3+} IN $R\text{CrO}_3$ ($R = \text{Nd}, \text{Ho}, \text{Er}$)

In the previous NES studies⁶⁻⁹ a cooperative ordering of the R^{3+} sublattice in $R\text{CrO}_3$ where $R = \text{Nd}, \text{Ho}, \text{Er}$ was reported, with $T_N \sim 10, 12,$ and 16 K, respectively. SMS studies on these compounds^{11,13,15} yielded ordering of the R^{3+} sublattice which is induced by the Cr^{3+} internal magnetic field. The temperature dependence of I_I , which is a pure R^{3+} magnetic reflection is presented in Fig. 9 for $R = \text{Nd}, \text{Ho}, \text{Er}$. The shape of these curves, mainly the concavity at high temperatures and the “abrupt” leveling off due to saturation at low temperature, is characteristic of induced ordering. Furthermore, the energy level

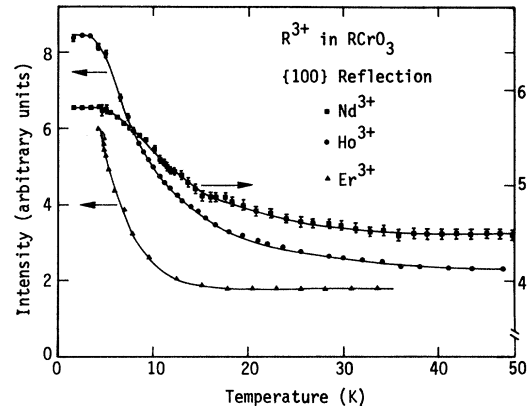


FIG. 9. Intensity vs temperature of the $\{100\}$ reflection (I_{II}) for $R = \text{Nd}, \text{Ho}, \text{Er}$ in $R\text{CrO}_3$. The solid lines are only guides to the eye. Where error bar is not indicated, the error is equal or smaller than the point dimension.

scheme of Ho^{3+} in HoCrO_3 was calculated²² using the Ho^{3+} magnetization curve from Fig. 9, assuming a Boltzmann-type population of the energy levels and a constant internal magnetic field. (The Cr^{3+} magnetic sublattice is nearly saturated in this temperature range, whereas a cooperative R^{3+} ordering would mean a strongly-temperature-dependent internal magnetic field). The energy-level values obtained by this calculation are in good agreement²² with those obtained by other methods. Hence, for HoCrO_3 we even have quantitative evidence that the R^{3+} magnetic order is induced by the Cr^{3+} sublattice in agreement with the SMS results.^{11,13,15}

IV. SUMMARY

Neutron ($\lambda \sim 2.4 \text{ \AA}$) elastic scattering measurements were conducted on those $R\text{CrO}_3$ compounds (where $R = \text{Pr}, \text{Nd}, \text{Ho}, \text{Er}, \text{Tm}, \text{Yb},$ and Lu) for which there were discrepancies in the magnetic structure determination between previous NES (which yielded mainly nonaxial structures) and SMS (which yielded axial structures) studies. A best fit of the calculated I_I/I_{II} , I_{III}/I_{IV} , and I_{II}/I_{III} to the observed values is presented in Table V assuming axial magnetic structures for all compounds. It can be seen that for $R = \text{Ho}, \text{Er}, \text{Yb}$ there is a good agreement, hence the present NES results concur with those of SMS. The calculated values of I_{III}/I_{IV} and the temperature dependence of I_{III} and I_{IV} indicate a negative sign between the Cr^{3+} and R^{3+} configurations (as defined in Table I and Fig. 1) in agreement with SMS. The previous neutron scattering measurements had not reported this sign change between the Cr^{3+} and R^{3+} configurations. The SMS and the present NES

results show (this is readily seen in the Ho, Tm, and Yb compounds, Table VI) that the R -Cr interaction is antiferromagnetic. The previous NES does not concur with this important result since the lack of sign change leads to ferromagnetic coupling between the ferromagnetic components of the R and Cr sublattices. For PrCrO_3 the possible directions of the sublattice magnetization of the Cr^{3+} ions were determined by symmetry considerations, through the Pr^{3+} sublattice magnetization direction determined by the existence of the $\{010\}$ and $\{100\}$ (unresolved) reflections. The existence of this reflection excludes the $[G_x; F_z]$ structure determined for PrCrO_3 by the previous neutron scattering measurements.¹⁴ The NdCrO_3 data also suffer from lack of resolution. However, adding symmetry arguments to the data we are able to deduce a structure in agreement with SMS. For TmCrO_3 the $I_{\text{III}}/I_{\text{IV}}$ value and the temperature dependences of I_{III} and I_{IV} can neither be explained by Tm contribution nor by Cr^{3+} spin reorientation. A temperature-dependent asphericity of the Cr^{3+} spin distribution can lead to agreement with these observations. We have, however, no physical explanation for such unusual behavior. LuCrO_3 is the only compound for which the present NES results seem to be consistent with the previous NES, and hence leads to a nonaxial magnetic structure. However, assuming a (temperature-independent) aspherical spin distribution of the Cr^{3+} ions, the NES results can yield the axial structure in agreement with the SMS structure. A magnetic moment of $2.2\mu_B$ was found for the Pr^{3+} ion by SMS while from the present NES measurements it is determined to be about 0.5 or $-0.6\mu_B$ (Table IV). We have no explanation for this discrepancy. We point out to the fact that single crystals were used in SMS and polycrystalline powder in NES. The present NES measurements indicate that the ordering of R^{3+} in the Nd, Ho, and Er compounds is not cooperative as reported by previous NES studies but is induced by the Cr^{3+} sublattice as reported by SMS studies.

APPENDIX: CALCULATIONS OF INTENSITY RATIOS OF MAGNETIC REFLECTIONS OF $R\text{CrO}_3$ FOR $[\text{Cr}; R]$ CONFIGURATIONS

The magnetic scattering is governed by the quantity²⁴

$$D \equiv |\hat{Q} \times (\vec{P} \times \hat{Q})|^2 = \vec{P}^2 - (\vec{P} \cdot \hat{Q})^2 ,$$

where \vec{P} is the magnetic scattering amplitude per unit cell and \hat{Q} is a unit vector perpendicular to the reflecting plane. The possible magnetic configurations are according to Table II. We simplify the calculations by assuming $c = \sqrt{2}b = \sqrt{2}a$. We also neglect the small Cr^{3+} moments, and we have $\Delta = hx + ky$.

(a) $[G_z; C_y, F_x]$ $\{011\}$

$$\frac{\vec{P}}{4} = [0, 0, S^{\text{Cr}}] + [0, S_y^R, 0] \sin \Delta = [0, S_y^R \sin \Delta, S^{\text{Cr}}] ,$$

$$\left(\frac{\vec{P}}{4} \cdot \hat{Q} \right)^2 = \left[[0, S_y^R \sin \Delta, S^{\text{Cr}}] \frac{[0, 1, 1/\sqrt{2}]}{\sqrt{3/2}} \right]^2 ,$$

$$\left(\frac{\vec{P}}{4} \right)^2 - \left(\frac{\vec{P}}{4} \cdot \hat{Q} \right)^2 = \frac{1}{3} (\sqrt{2} S^{\text{Cr}} - S_y^R - S_y^R \sin \Delta)^2 , \quad (\text{A1})$$

$\{101\}$

$$\left(\frac{\vec{P}}{4} \right)^2 - \left(\frac{\vec{P}}{4} \cdot \hat{Q} \right)^2 = \frac{1}{3} (\sqrt{2} S^{\text{Cr}} - S_x^R \sin \Delta)^2 , \quad (\text{A2})$$

hence

$$\frac{D(011)}{D(101)} = \left(\frac{\sqrt{2} S^{\text{Cr}} - S_y^R \sin \Delta}{\sqrt{2} S^{\text{Cr}} - S_x^R \sin \Delta} \right)^2 . \quad (\text{A3})$$

(b) $[G_y; C_z]$ $\{011\}$

A similar calculation leads to

$$\left(\frac{\vec{P}}{4} \right)^2 - \left(\frac{\vec{P}}{4} \cdot \hat{Q} \right)^2 = \frac{1}{3} (S^{\text{Cr}} - \sqrt{2} S^R \sin \Delta)^2 , \quad (\text{A4})$$

$\{101\}$

$$\frac{\vec{P}}{4} = [0, S^{\text{Cr}}, 0] ,$$

and

$$\left(\frac{\vec{P}}{4} \cdot \hat{Q} \right)^2 = \left[[0, S^{\text{Cr}}, 0] \frac{[1, 0, 1/\sqrt{2}]}{\sqrt{3/2}} \right]^2 = 0 ,$$

hence

$$\frac{D(011)}{D(101)} = \frac{1}{3} \left(\frac{S^{\text{Cr}} - \sqrt{2} S^R \sin \Delta}{S^{\text{Cr}}} \right)^2 . \quad (\text{A5})$$

(c) $[G_x; F_x]$ $\{011\}$

$$\frac{\vec{P}}{4} = [S^{\text{Cr}}, 0, 0] \text{ and } \left(\frac{\vec{P}}{4} \cdot \hat{Q} \right)^2 = 0 ,$$

$\{101\}$

$$\left(\frac{\vec{P}}{4} \right)^2 - \left(\frac{\vec{P}}{4} \cdot \hat{Q} \right)^2 = \frac{1}{3} (S^{\text{Cr}} - \sqrt{2} S^R \sin \Delta)^2 , \quad (\text{A6})$$

hence

$$\frac{D(011)}{D(101)} = 3 \left(\frac{S^{\text{Cr}}}{S^{\text{Cr}} - \sqrt{2} S^R \sin \Delta} \right)^2 . \quad (\text{A7})$$

The intensity of magnetic reflection from a powder sample is given by²³

$$I_{\text{calc}}^{\text{mag}} = A \frac{j D f^2}{\sin \theta \sin 2\theta} ,$$

where A is a geometric factor depending on the experimental layout, j the multiplicity of the reflection, and 2θ is the scattering angle. We label $\{010\}$, $\{100\}$, $\{011\}$, and $\{101\}$ by I, II, III, and IV (in order of in-

creasing 2θ), respectively. We obtain

[$G_z; C_y, F_x$]

$$\frac{I_{III}}{I_{IV}} = \left(\frac{\sqrt{2}f_{III}^{Cr}S^{Cr} - f_{III}^R S_y^R \sin\Delta_{III}}{\sqrt{2}f_{IV}^{Cr}S^{Cr} - f_{IV}^R S_x^R \sin\Delta_{IV}} \right)^2 \frac{\sin\theta_{IV}\sin 2\theta_{IV}}{\sin\theta_{III}\sin 2\theta_{III}}, \quad (A8)$$

[$G_y; C_z$]

$$\frac{I_{III}}{I_{IV}} = \frac{1}{3} \left(\frac{f_{III}^{Cr}S^{Cr} - \sqrt{2}f_{III}^R S^R \sin\Delta_{III}}{f_{IV}^{Cr}S^{Cr}} \right)^2 \frac{\sin\theta_{IV}\sin 2\theta_{IV}}{\sin\theta_{III}\sin 2\theta_{III}}, \quad (A9)$$

[$G_x; F_z$]

$$\frac{I_{III}}{I_{IV}} = 3 \left(\frac{f_{III}^{Cr}S^{Cr}}{f_{IV}^{Cr} - \sqrt{2}f_{IV}^R S^R \sin\Delta_{IV}} \right)^2 \frac{\sin\theta_{IV}\sin 2\theta_{IV}}{\sin\theta_{III}\sin 2\theta_{III}}. \quad (A10)$$

The I_I and I_{II} have only R^{3+} magnetic contribution. A straightforward calculation yields

[$G_z; C_y, F_x$]

$$I_I = 0, \quad I_{II} = A \frac{j(4f_{II}^R S_y^R \cos\Delta_{II})^2}{\sin\theta_{II}\sin 2\theta_{II}},$$

[$G_y; C_z$]

$$\frac{I_I}{I_{II}} = \left(\frac{f_I^R \cos\Delta_I}{f_{II}^R \cos\Delta_{II}} \right)^2 \frac{\sin\theta_{II}\sin 2\theta_{II}}{\sin\theta_I\sin 2\theta_I}, \quad (A11)$$

[$G_x; F_z$]

$$I_I = I_{II} = 0.$$

¹S. Geller and E. A. Wood, *Acta Crystallogr.* **9**, 563 (1956).

²These configurations transform as irreducible representations of the paramagnetic space group $1'Pbnm$ with $\vec{k} = 0$.

³E. W. Wollan and W. C. Koehler, *Phys. Rev.* **100**, 545 (1955).

⁴E. F. Bertaut, in *Magnetism*, edited by G. T. Rado and H. Suhl (Academic, New York, 1963), Vol. III.

⁵These structures transform as irreducible representations of the paramagnetic space group $1'Pbnm$ with $\vec{k} = 0$.

⁶E. F. Bertaut, G. Buisson, A. Delapalme, B. Van Laar, R. Lemaire, J. Mareschal, G. Rault, J. Schwitzer, Vu Van Qui, H. Bartolin, M. Mercier, and R. Pauthenet, 1964 Proceedings of the International Conference on Magnetism (unpublished), p. 275.

⁷E. F. Bertaut, J. Mareschal, G. De Vries, R. Alenard, R. Pauthenet, J. P. Rebouillat, and V. Zarubicka, *IEEE Trans. Magn.* **2**, 453 (1966).

⁸E. F. Bertaut and J. Mareschal, *Solid State Commun.* **5**, 93 (1967).

⁹P. Pataud and J. Sivardiere, *J. Phys. (Paris)* **31**, 803 (1970).

¹⁰S. Shtrikman, B. M. Wanklyn, and I. Yaeger, *Int. J. Magn.* **1**, 327 (1971).

¹¹R. M. Hornreich, B. M. Wanklyn, and I. Yaeger, *Int. J. Magn.* **2**, 77 (1972).

¹²R. M. Hornreich, B. M. Wanklyn, and I. Yaeger, *Int. J. Magn.* **4**, 313 (1973).

¹³R. M. Hornreich, Y. Komet, R. Nolan, B. M. Wanklyn, and I. Yaeger, *Phys. Rev. B* **12**, 5094 (1975).

¹⁴J. D. Gordon, R. M. Hornreich, S. Shtrikman, and B. M. Wanklyn, *Phys. Rev. B* **13**, 3012 (1976).

¹⁵A. Hasson, R. M. Hornreich, Y. Komet, B. M. Wanklyn, and I. Yaeger, *Phys. Rev. B* **12**, 5051 (1975).

¹⁶R. M. Hornreich, S. Shtrikman, B. M. Wanklyn, and I. Yaeger, *Phys. Rev. B* **13**, 4046 (1976).

¹⁷A. J. Freeman and R. E. Watson, *Acta Crystallogr.* **14**, 231 (1961).

¹⁸R. M. Moon, W. C. Kohler, and A. L. Trego, *J. Appl. Phys.* **37**, 1036 (1966).

¹⁹G. P. Felcher, G. H. Lander, T. Arai, S. K. Sinha, and F. H. Spedding, *Phys. Rev. B* **13**, 3034 (1976).

²⁰M. Marezio, J. P. Remeika, and P. D. Dermier, *Acta Crystallogr. Sect. B* **26**, 2008 (1970).

²¹Z. Fridman, H. Pinto, H. Shaked, G. Gorodetsky, and S. Shtrikman, *Int. J. Magn.* **2**, 409 (1971).

²²N. Shamir, H. Shaked, and S. Shtrikman, *Physica* **90B**, 211 (1977), and references therein.

²³G. E. Bacon, *Neutron Diffraction*, 3rd ed. (Oxford University Press, Cambridge, England, 1975).